NeuroImage 191 (2019) 225–233

Contents lists available at ScienceDirect

NeuroImage

journal homepage: www.elsevier.com/locate/neuroimage

Desynchronizing to be faster? Perceptual- and attentional-modulation of brain rhythms at the sub-millisecond scale

Yasuki Noguchi [a,*], Yi Xia [a], Ryusuke Kakigi [b]

[a] Department of Psychology, Graduate School of Humanities, Kobe University, 1-1 Rokkodai-cho, Nada, Kobe, 657-8501, Japan
[b] Department of Integrative Physiology, National Institute for Physiological Sciences, 38 Nishigonaka, Myodaiji, Okazaki, 444-8585, Japan

ARTICLE INFO

Keywords:
Event-related desynchronization (ERD)
Neural periodicity
Posner spatial cuing task
Inhibitory control
Alpha blocking

ABSTRACT

Neural oscillatory signals has been associated with many high-level functions (e.g. attention and working memory), because they reflect correlated behaviors of neural population that would facilitate the information transfer in the brain. On the other hand, a decreased power of oscillation (event-related desynchronization, ERD) has been associated with an irregular state in which many neurons behave in an uncorrelated manner. In contrast to this view, here we show that the human ERD is linked to the increased regularity of oscillatory signals. Using magnetoencephalography, we found that presenting a visual stimulus not only induced a decrease in power of alpha (8–12 Hz) to beta (13–30 Hz) rhythms in the contralateral visual cortex but also reduced the mean and variance of their inter-peak intervals (IPIs). This indicates that the suppressed alpha/beta rhythms became faster (reduced mean) and more regular (reduced variance) during visual stimulation. The same changes in IPIs, especially those of beta rhythm, were observed when subjects allocated their attention to a contralateral visual field. Those results revealed a new role of the event-related decrease in alpha/beta power and further suggested that our brain regulates and accelerates a clock for neural computations by actively suppressing the oscillation amplitude in task-relevant regions.

1. Introduction

Many studies suggest that neural oscillatory signals could serve various important functions in the brain. Unit-cell recordings on animals showed that changes in amplitude and coherence of gamma-band oscillation are strongly linked to cognitive processes such as feature integration and attention (Engel et al., 2001; Fries, 2009), while oscillations in theta-band plays a key role in memory (Buzsaki and Moser, 2013; Knyazev, 2007). The close relationships between oscillatory signals and cognitive functions have been also demonstrated in the human brain (Jensen et al., 2007; Palva and Palva, 2011). In electroencephalography (EEG) and magnetoencephalography (MEG), an increase in power of a given frequency band is called the event-related synchronization (ERS), which reflects cooperative or synchronized behaviors of a large number of neurons (Pfurtscheller and Lopes da Silva, 1999) that would facilitate the information transfer across neuronal groups (Fries, 2005). Consistent with this view, a spatial allocation of attention induced the gamma-band ERS in the sensory cortex of a contralateral hemisphere (Bauer et al., 2006), and stronger theta-band ERS in a memory encoding stage predicted better performances in later retrieval stage (Osipova et al., 2006).

In contrast to the ERS, a decrease in power of oscillatory signals is called the event-related desynchronization or ERD (Pfurtscheller and Lopes da Silva, 1999), being associated with uncorrelated (irregular) behaviors of neural population. Paradoxically, many studies have reported the ERD in brain regions that would play a central role in a given task (task-relevant regions). A well-known example is the alpha ERD over the occipital cortex in response to visual inputs (Berger, 1929). Recent studies showed that not only the alpha rhythm (8–12 Hz) but also the beta rhythm (13–30 Hz) showed prominent ERD to visual (Kulashekhar et al., 2016; Minami et al., 2014; Wyart and Tallon-Baudry, 2009), auditory (Cirelli et al., 2014; de Pesters et al., 2016; Fujioka et al., 2015), and somatosensory (Bauer et al., 2006; Fransen et al., 2016) stimuli. The alpha/beta ERD in the sensory areas was also induced by attention (van Ede et al., 2012). A voluntary allocation of attention to a visual hemifield reduced alpha/beta power in the contralateral visual cortex (Bauer et al., 2014; Worden et al., 2000; Wyart and Tallon-Baudry, 2009).

Why was the ERD, a neural signature of uncorrelated activities, observed in task-relevant regions? Previous studies resolved this issue by assuming an inhibitory role of alpha oscillation on neural processing (Jensen and Mazaheri, 2010; Klimesch, 2012). For example, Jensen and

* Corresponding author.
E-mail address: ynoguchi@lit.kobe-u.ac.jp (Y. Noguchi).

https://doi.org/10.1016/j.neuroimage.2019.02.027
Received 25 August 2018; Received in revised form 14 January 2019; Accepted 11 February 2019
Available online 14 February 2019

Mazaheri (2010) argued that alpha activity provides pulsed inhibition reducing the processing capabilities of a given area. A recent study also reported the inhibitory role of beta rhythm on neural processing (Shin et al., 2017). The alpha/beta ERD observed in task-relevant regions thus would reflect a release from this periodic (regular) inhibition, representing the active processing of sensory information in a contra-stimulus and contra-attention hemisphere.

Although this release-from-inhibition (disinhibition) hypothesis of alpha/beta ERD is widely accepted, here we explore a new role of ERD other than the disinhibition. Specifically, we focused on changes in *frequency* (Cohen, 2014) and *regularity* (Fransen et al., 2015) of neural rhythms caused by the ERD. Regularity (or periodicity) is one of the most fundamental information in oscillatory signals. Indeed, previous studies reported altered regularity of neural oscillations in patients with mental disorders such as Alzheimer's disease (Gomez et al., 2007; Poza et al., 2012). We hypothesized that, if the alpha/beta ERD represents weakened (less-regulated) pulses of inhibition, this would be associated with decreased regularity of oscillations in the same frequency band.

Basic procedures of our MEG experiment are shown in Fig. 1. Participants performed the standard Posner task in which their attention was directed to either a left or right visual field (Fig. 1A). A central cue (arrow) and a peripheral task stimulus (Gabor patch) would induce a decrease in alpha/beta power in a contralateral (contra-attention and contra-stimulus) hemisphere. To quantify the regularity, we measured inter-peak intervals (IPIs) of oscillatory signals (Fig. 1B), depicting a distribution of their occurrences (Fig. 1C). For example, an IPI distribution of alpha rhythm (8–12 Hz) would be centered on 100 ms, because its central frequency is 10 Hz. When the alpha rhythm is highly regular, most IPIs would be located around the mean (100 ms), which results in a smaller variance of the distribution (Fig. 1C, top). In contrast, an irregular alpha wave would be indexed by a large variance because such irregular rhythm produces IPIs distant from 100 ms (Fig. 1C, bottom). One advantage of our method is that it can measure various types of changes in oscillatory signals simultaneously. For example, if the decreased alpha/beta power causes an overall increase in an oscillation frequency, this would be detected as a decrease in a mean (rather than variance) of IPIs.

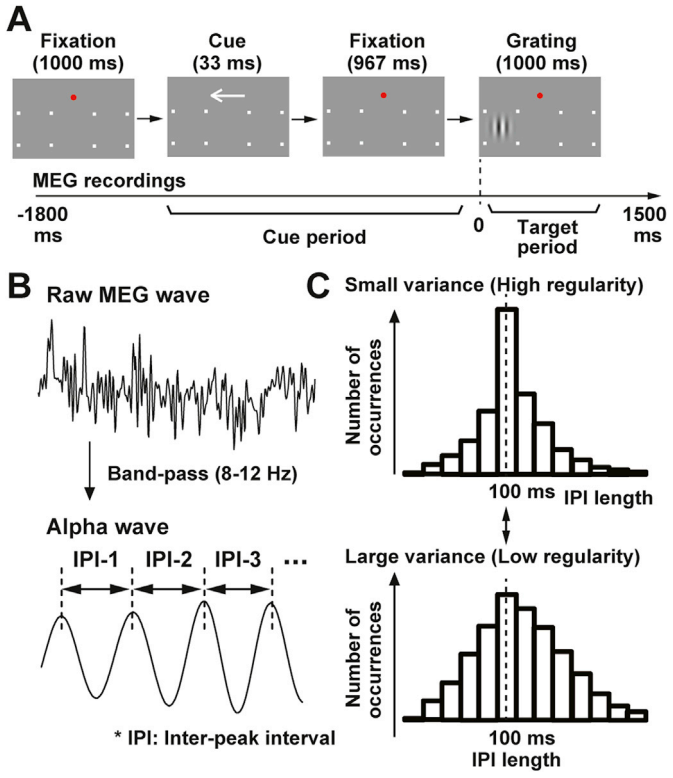

Fig. 1. Experimental procedures. (**A**) Structures of one trial. A central cue (arrow) guided attention of subjects into either left visual field (LVF) or right visual field (RVF). Subjects pressed a button only when a grating with a target orientation (vertical or horizontal, variable across subjects) was presented at an attended hemifield. No response was required to a grating with a non-target orientation or a grating at an unattended hemifield. (**B**) Schematic illustrations of the inter-peak interval (IPI) analysis in the present study. First, oscillatory signals with a frequency band of interest (e.g. 8–12 Hz) were extracted with a band-pass filter. An IPI was defined as a time length between contiguous peaks of the filtered waveform. All IPIs within a period of interest (e.g. cue period) were pooled across trials. (**C**) Distributions of IPIs across all trials. The mean of the distribution should be around 100 ms (dotted line), because a central frequency of a pass band (8–12 Hz) is 10 Hz. When oscillatory signals are highly regular, most IPIs would be located around the mean (upper panel). In contrast, an irregular alpha wave would produce many IPIs distant from the mean (lower panel). The irregularity of oscillatory signals can be thus indexed by a standard deviation (SD) of an IPI distribution.

2. Materials and methods

2.1. Participants

Twenty-two healthy human subjects (13 females, age: 20–54) participated in the present study. Informed consent was received from each participant after the nature of the study had been explained. All experiments were carried out in accordance with guidelines and regulations approved by the ethics committee of Kobe University, Japan.

2.2. Stimuli and task

We used the Matlab Psychophysics Toolbox (Brainard, 1997; Pelli, 1997) to generate visual stimuli (refresh rate: 60 Hz) and to record button-press responses by participants. Each trial started with a screen of a red fixation point (0.19 × 0.19 deg) for 1000 ms (Fig. 1A). This fixation screen also had place holders (four white dots), one set in the lower left visual field (LVF) and the other set in the lower right visual field (RVF), indicating possible locations of an upcoming task stimulus (grating). To direct attention of participants, we then presented a cue stimulus (an arrow pointing leftward or rightward, 1.375 deg) over the central visual field for 33 ms, which was followed by another fixation screen for 967 ms. Finally, a grating with a vertical or horizontal orientation (size: 2 × 2 deg, center-to-fixation distance: 4.2 deg) was presented as a task stimulus either in LVF or RVF for 1000 ms. The next trial began after the fixation screen of 800 ms (inter-trial interval). Participants were asked to move their attention covertly into a cued location, pressing a button as quickly as possible by their right hand when a grating with a target orientation (target grating) appeared there. The target orientation was vertical for a half of participants (N = 11) and horizontal for the other half (N = 11). They were also instructed to suppress the button-press response to a non-target grating in an attended hemifield and to totally ignore all gratings in an unattended hemifield.

A combination of a cued hemifield (left/right) and a position of the task stimulus (left/right) produced four types of trials: left cue & left stimulus (LL), left cue & right stimulus (LR), right cue & left stimulus (RL), right cue & right stimulus (RR). An experimental session comprised 72 trials in which those four types of trials (18 for each) were randomly intermixed (Fig. 2). A ratio of target and non-target gratings was 3:15, meaning that participants should press the button for six times per session (three times for LL trials and three times for RR trials). Each participant underwent five sessions.

2.3. MEG recordings

Neural activity was recorded with a whole-head MEG system (Vectorview, ELEKTA Neuromag, Helsinki, Finland). This system measured neuromagnetic signals from 102 positions over the scalp using 204

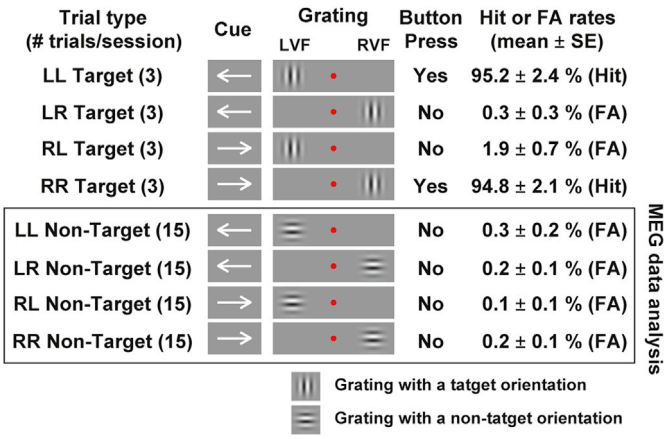

Fig. 2. A list of all trial types. Numbers in parentheses indicate numbers of trials per experimental session. The grating with a vertical orientation is shown as a target in this figure. A hit or false-alarm (FA) rate for each trial type is shown in the right column (mean SE ± across participants). All analyses on MEG data were performed on the non-target trials (from LL Non-Target to RR Non-Target).

planer-type sensors (two sensors per recording position). One sensor measured latitudinal directions of changes in neuromagnetic signals while the other measured changes in longitudinal directions (sampling rate: 4 kHz, analogue band-pass filter: 0.1–330 Hz). Data from those two sensors at the same recording position were integrated in later analyses (see below). The MEG waveforms measured through those planar gradiometers represent neural activity in the cerebral cortex just below the recording position (Nishitani and Hari, 2002). Other details were shown in our previous publications (Noguchi et al., 2015; Suzuki et al., 2014).

The preprocessing of MEG data were performed with the Brainstorm toolbox for Matlab (Tadel et al., 2011). First, neuromagnetic signals were segmented and classified into four conditions (LL, LR, RL, and RR). An epoch for the segmentation ranged from −1800 to 1500 ms relative to an onset of a task stimulus (Fig. 1A). Data in a pre-stimulus (post-cue) period from −1000 to 0 ms were used to investigate changes in oscillatory signals related to an allocation of attention, while changes related to visual perception were investigated in a post-stimulus (target) period from 0 to 1000 ms. Trials in which a signal variation (a difference between maximum and minimum values within a period of −1200 to 1000 ms) was larger than 4500 fT/cm were excluded from further analyses. We also discarded trials in which a target grating was presented, because waveforms in those target trials contained noises resulting from manual button-press movements.

2.4. Power analysis

We first analyzed changes in power of oscillatory signals over time, to confirm the attention- and perception-related decrease in alpha/beta power in previous studies (Bauer et al., 2014; Kulashekhar et al., 2016; Minami et al., 2014; Worden et al., 2000; Wyart and Tallon-Baudry, 2009). A time-frequency (TF) transform using complex Morlet wavelets was applied to the segmented MEG data of non-target trials (central frequency: 1 Hz, time resolution at full width at half maximum: 3 s), which converted an MEG waveform into a power spectrum of time (−1800 to 1500 ms) × frequency (1–100 Hz). Those TF spectra were then averaged across all trials and between latitudinal and longitudinal sensors at each recording position. To measure relative changes in power over time, we performed a baseline correction of the TF data. For each frequency, all data from −1500 to 1800 ms were converted into decibel (dB) change from a baseline, as shown by

$$y = 10 \times \log10(x/u)$$

, where x and y indicate powers before and after the baseline correction, and u indicates a mean power over a baseline period. The baseline period was set at −1200 to −1000 ms when we investigated power changes in the cue period (Fig. 3) and set at −200 to 0 ms when investigating changes in the target period (Fig. 6).

2.5. Source estimation

We estimated anatomical source locations of alpha suppression (Fig. 6D) with the minimum norm (MN) approach in the Brainstorm toolbox. First, a spherical head model of each subject was constructed, using positional information of MEG sensors and a template brain of the Montreal Neurological Institute. This model for forward solutions was then inverted with the MN approach, which converted neuromagnetic waveforms at 204 sensors into a 4D current density map (cortical activation map) of multiple dipoles placed over the cortical surface. Finally, those changes in the current density over time were transformed into power spectrum with the Welch's method (power density map). Noise covariance matrix for those MN estimations was computed using MEG signals in a pre-cue baseline period (−1200 to −1000 ms).

For second-level (group-level) analyses across 22 subjects, the power density map of each subject was exported to Statistic Parametric Mapping (SPM) 12. Brain regions showing the alpha suppression to a contralateral task stimulus were estimated by the random-effect analysis (voxel-wise *t*-tests) comparing Stimulus-Left condition (average of LL and RL trials, expressed as "LL + RL" hereafter) and Stimulus-Right condition ("LR + RR").

2.6. Inter-peak interval analysis

We evaluated changes in speed and regularity of oscillation signals using the inter-peak interval (IPI) analysis. First, we decomposed raw MEG waveforms into six bands of frequency (delta: 2–4 Hz, theta: 5–7 Hz, alpha: 8–12 Hz, beta: 13–30 Hz, gamma: 31–59 Hz, and high-gamma: 60–100 Hz) using the zero-phase Butterworth filters (order: 3). The filter of a broader pass-band (8–30 Hz) was also used, because previous studies reported the wide-band ERD covering an alpha-to-beta range (Bauer et al., 2014; Minami et al., 2014). For each of the filtered waveform, we identified peaks of oscillatory signals and measured intervals between contiguous peaks (IPIs). All IPIs within a period of interest (e.g. cue period) were then pooled across trials. Finally, we computed four parameters of an IPI distribution (Fig. 1C); mean, standard deviation (SD), median, and coefficient of variation (CV). The CV is the SD divided by the mean IPI, which represents the irregularity (variance) of neural signals normalized to a mean (Taube, 2010). A higher CV indicates lower regularity of signals. Those statistical measures of IPIs were averaged between latitudinal and longitudinal sensors at each recording position.

2.7. Statistical analysis

A purpose of the present study was to measure changes in oscillatory signals related to perception and attention. An effect of attention was investigated using the data in the cue period. For each of 102 sensor positions, data in Attend-Left condition (LL + LR) were compared with those in Attend-Right condition (RL + RR) by a paired *t*-test (N = 22). Resultant *t*-maps over a spatial layout of 102 sensor positions were shown in Figs. 3 and 4. For example, attention-related suppression of alpha power (Bauer et al., 2014; Worden et al., 2000; Wyart and Tallon-Baudry, 2009) was shown in upper right panel in Fig. 3D. The Attend-Right condition induced the suppression of alpha power in the contralateral left hemisphere (Attend-L > Attend-R, colored in red), while the Attend-Left condition induced alpha suppression in the right hemisphere (Attend-L < Attend-R, blue). A problem of multiple comparisons (caused by a repetition of *t*-test at 102 sensor positions) was resolved by controlling false discovery rate (FDR). For each *t*-map, a statistical threshold was adjusted for multiple testing with Benjamini-Hochberg correction (Benjamini and Hochberg, 1995) with the *q*-value set at < 0.05. Sensors

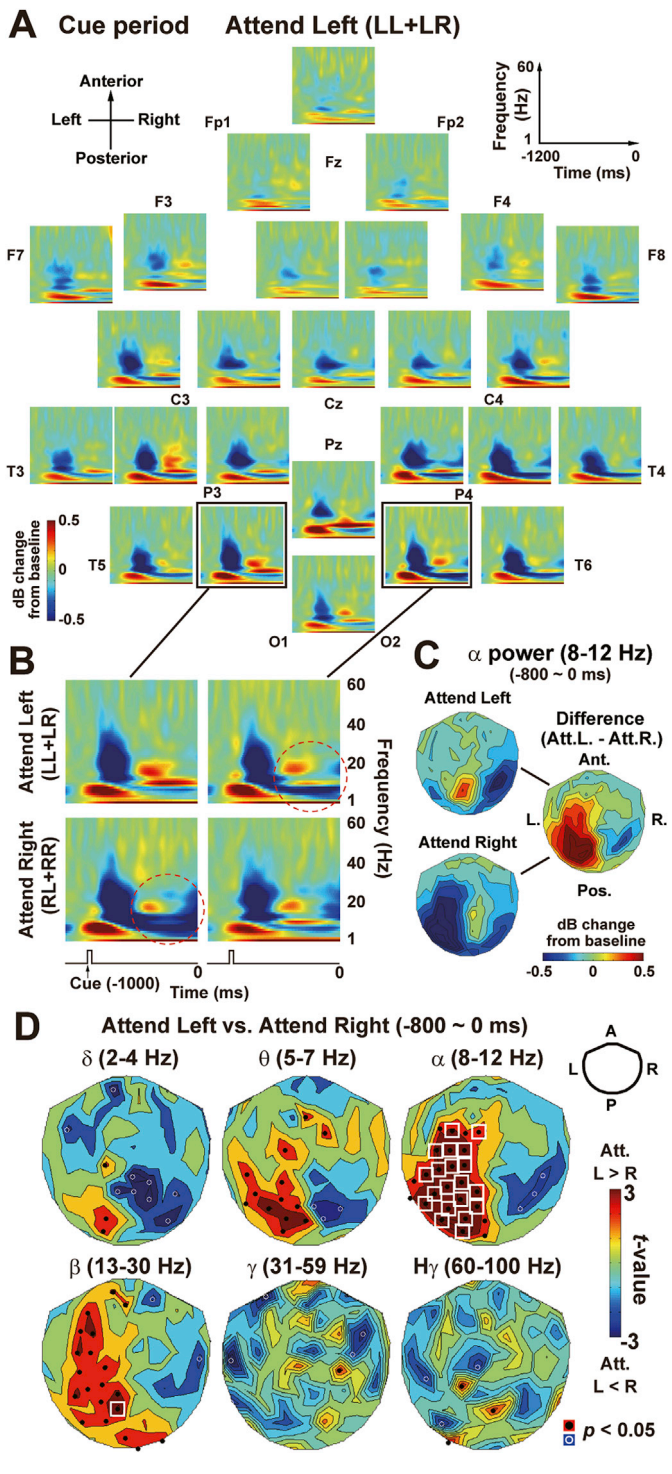

(caption on next column)

Fig. 3. Results of the power analysis in the cue period. (**A**) Changes in power of oscillatory signals (1–60 Hz, vertical axis) over time (−1200 to 0 ms, horizontal axis) when subjects attended to LVF. Red and blue indicate an increase and decrease in power relative to a baseline period (−1200 to −1000 ms), respectively. We classified time-frequency (TF) spectra at 102 sensor positions into 26 groups (areas), with all spectra within the same group averaged together (areal-mean spectra). Approximate positions of the 26 areas are indicated by labels in the international 10–20 system (e.g. Cz). (**B**) Areal-mean spectra over the left and right visual regions in Attend-Left (upper panels) and Attend-Right (lower panels) conditions. Attending to LVF (RVF) suppressed alpha power over the right (left) visual cortex (dotted red circles). (**C**) Contour maps of alpha power over 102 sensor positions. A differential contour map (Attend-Left minus Attend-Right) was characterized by an increase (decrease) in alpha power in the left (right) visual cortex. (**D**) Statistical *t*-maps over 102 sensor positions. For each of six frequency bands from delta to high-gamma, oscillation powers are compared between Attend-Right and Attend-Left conditions. Black dots and white circles indicate sensors showing a significant ($p < 0.05$) difference. White rectangles denote sensors with a significant difference after a correction of multiple comparisons. A clear decrease in alpha power was observed in the contra-attention hemisphere (upper right). Similar patterns were also seen in delta, theta, and beta bands.

with a significant difference after this correction were indicated by white rectangles.

We then investigated changes in powers and IPIs related to visual perception (Figs. 6 and 7). Data in Stimulus-Left condition (LL + RL) were compared with Stimulus-Right condition (LR + RR). Other procedures (sensor-space *t*-map and correction of multiple comparisons, etc.) were the same as those on attention-related changes.

3. Results

3.1. Behavioral data

Hit and false-alarm (FA) rates in all types of trials (mean ± SE across participants) are shown in Fig. 2. Participants correctly pressed a button when a grating with a target orientation (target grating) appeared in an attended visual field (hit rates: 95.2% in LL target and 94.8% in RR target trials). Reactions times measured from an onset of a grating were 665.9 ± 23.6 ms (LL) and 665.7 ± 22.2 ms (RR). No difference in hit rates ($t(21) = 0.30$, $p = 0.77$, Cohen's $d = 0.029$) or reaction times ($t(21) = 0.02$, $p = 0.98$, Cohen's $d = 0.002$) was observed between LL target and RR target trials. On the other hand, the FA rates for a target grating presented in an unattended visual field were 0.3% (LR) and 1.9% (RL), which indicated that participants directed their attention following an instruction of the cue. The FA rates to a non-target grating were generally low, ranging from 0.1 to 0.3%.

3.2. Oscillatory powers and IPIs in the cue period

Fig. 3A shows TF (time-frequency) spectra around the cue period (−1200 to 0 ms) when participants directed their attention into LVF (an average of LL and LR trials, expressed as "LL + LR" hereafter). See also Fig. S1 (Supplementary Materials) for a power spectrum for each subject. To obtain an overview of all 102 sensor positions, we classified those into 26 areas (25 areas of four sensor positions plus one area of two sensor positions). Spectra at four (or two) positions within each area were averaged together (areal-mean analyses (Suzuki et al., 2014)). Consistent with previous studies (Bauer et al., 2014; Worden et al., 2000; Wyart and Tallon-Baudry, 2009), an allocation of attention induced continuous suppression of alpha power (8–12 Hz) in a contralateral hemisphere (Fig. 3B and C). Statistical comparisons of powers between Attend-Left (LL + LR) and Attend-Right (RL + RR) conditions (sensor-space *t*-maps, Fig. 3D) revealed the attention-related decrease in the contralateral hemisphere not only in alpha rhythm but also in delta (2–4 Hz), theta (5–7 Hz), and beta (13–30 Hz) rhythms.

We then computed IPIs of the six frequency bands and compared them between Attend-Left and Attend-Right conditions. As shown in the lower left panel in Fig. 4A, an effect of attention on IPI lengths was prominent in the beta band. Attending to LVF reduced the mean IPI length over the right visual cortex (Attend L < R, colored in blue), while attending to RVF reduced the IPIs over the left visual cortex (Attend L > R, colored in red). The same results were obtained when we analyzed IPIs of alpha-to-beta rhythms using a band-pass filter of 8–30 Hz

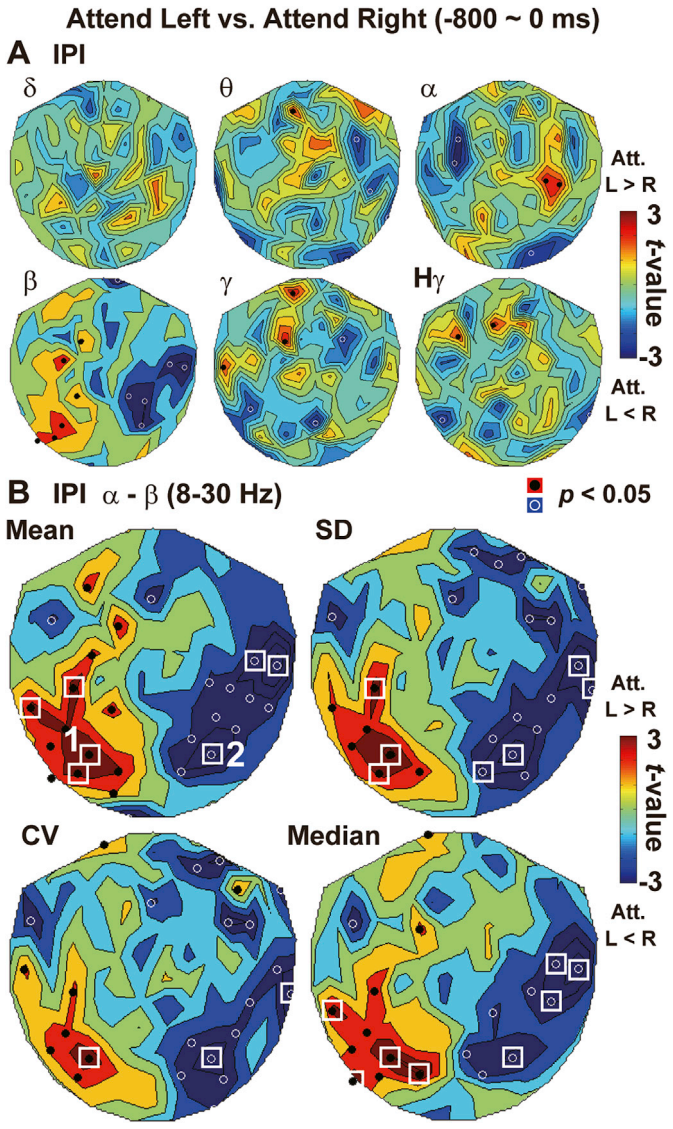

Fig. 4. Results of the IPI analysis in the cue period. (**A**) Sensor-space *t*-maps comparing mean IPIs between Attend-Left and Attend-Right conditions, separately computed for the six frequency bands. (**B**) Sensor-space *t*-maps of IPIs in the alpha-to-beta band (8–30 Hz). Four measures of an IPI distribution (mean, SD, coefficient of variation, and median) were compared between Attend-Left and Attend-Right conditions. The coefficient of variation (CV) is the SD divided by the mean IPI, which represents the irregularity of neural signals (Taube, 2010). A lower CV indicates higher regularity of signals.

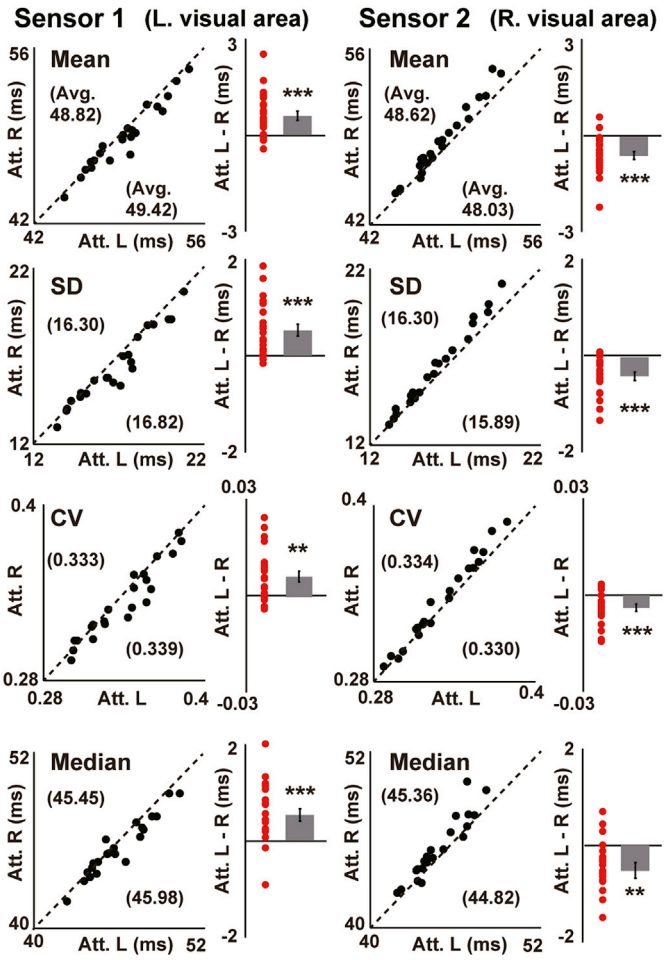

Fig. 5. Data of individual subjects at representative sensors (Sensor 1 over the left visual area and Sensor 2 over the right visual area, see Fig. 4B). For each of four IPI measures (mean, SD, CV, and median), individual data (N = 22) in Attend-Left (*x*) and Attend-Right (*y*) conditions are shown on two-dimensional plots with 45-deg line (black dots). Averages (Avg.) across the 22 participants are shown in parentheses. Red dots denote between-condition differences (Attend L – Attend R) with their mean ± SE shown as the bar graph. The IPI became shorter (mean and median) and more regular (SD and CV) in the contra-attention hemisphere. $^{**}p < 0.01$, $^{***}p < 0.001$.

(Fig. 4B). Individual data (N = 22) in alpha-to-beta IPIs at two representative sensors are shown in two-dimensional plots in Fig. 5. In the left hemisphere (Sensor 1, see Fig. 4B), most black dots were located below a diagonal (45-deg) line, indicating that IPIs in Attend-Right condition were shorter than those in Attend-Left condition. Differences of mean IPI (Attend L - R) were thus positive in most participants (red dots). These patterns were reversed in the right hemisphere (Sensor 2) in which mean IPI was shorter in Attend-Left than Attend-Right conditions.

Attention-related changes in SD of IPIs are shown in the upper right panel in Fig. 4B. We found a significant decrease in SD in the contra-attention hemisphere, indicating that neural oscillations in alpha-to-beta band became more periodic by an allocation of attention to a contralateral visual field. Regularity of oscillatory signals was further evaluated by CV (coefficient of variation), which was the SD divided by the mean. Significant decreases in the contra-attention hemisphere (Fig. 4B, lower left) showed that attention not only induced the alpha/beta power but also enhanced the regularity of neural rhythms in the same regions. Although a previous study reported an increase in entropy (a decrease in regularity) of gamma rhythm (>30 Hz) during alpha desynchronization (Werkle-Bergner et al., 2014), this was not confirmed in the present IPI analysis (data not shown).

One possible reason for the attention-related decrease in mean IPI is an inhibition of transient events in oscillatory signals. It is widely known that high-power oscillation in a given frequency (e.g. 14 Hz) can emerge intermittently in neural waveforms (e.g. spindles and beta burst) (Shin et al., 2017). Such transient events might produce IPIs far longer than average (outlier IPIs). The mean IPI in the contra-attention visual cortex became shorter (Fig. 4B) because the decreased alpha/beta power in this region (Fig. 3D) might prevent an emergence of those transient bursts, thereby eliminating the outlier IPIs. To examine this possibility, we computed a median of an IPI distribution, a statistical measure less influenced by outliers. Results revealed an attention-related decrease in the contralateral hemisphere (the lower right panel in Fig. 4B), which suggests that the shortening of IPIs took place as a whole (not resulting from the elimination of outliers). Our results thus cannot be explained by

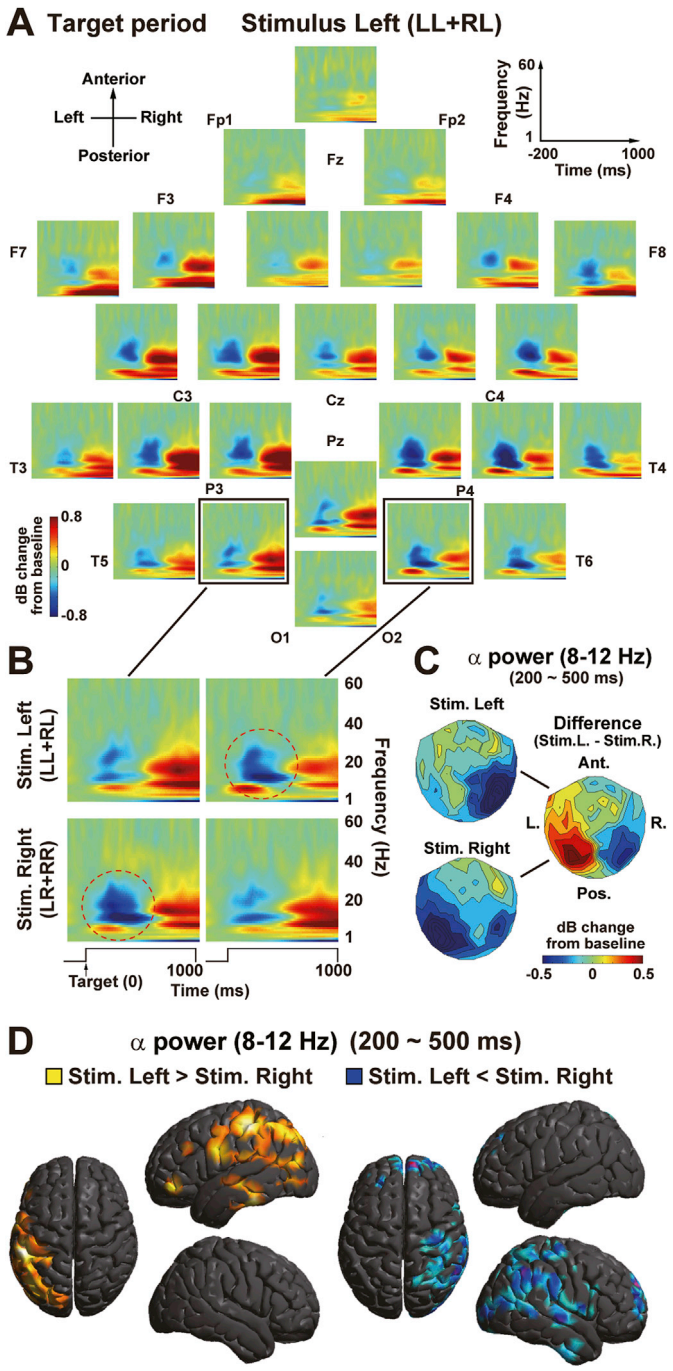

Fig. 6. Results of power analysis in the target period. (**A**) Areal-mean spectra when a grating was presented at LVF (Stimulus-Left conditions). (**B**) Enlarged TF spectra over the bilateral visual regions. Presenting a stimulus predominantly suppressed alpha power over the contralateral visual region (dotted circles). (**C**) Contour maps of alpha power over 102 sensor positions. Mean power in a time window of 200–500 ms are compared between Stimulus-Left and Stimulus-Right conditions. A differential map (Stimulus-Left minus Stimulus-Right) was characterized by an increase and decrease in alpha power in the left and right visual regions, respectively. (**D**) Anatomical source locations for the decrease in alpha power (estimated by SPM12). Regions with decreased alpha power in Stimulus-Right conditions are found in the left hemisphere (left panels), while those in Stimulus-Left conditions are seen in the right hemisphere (right panels).

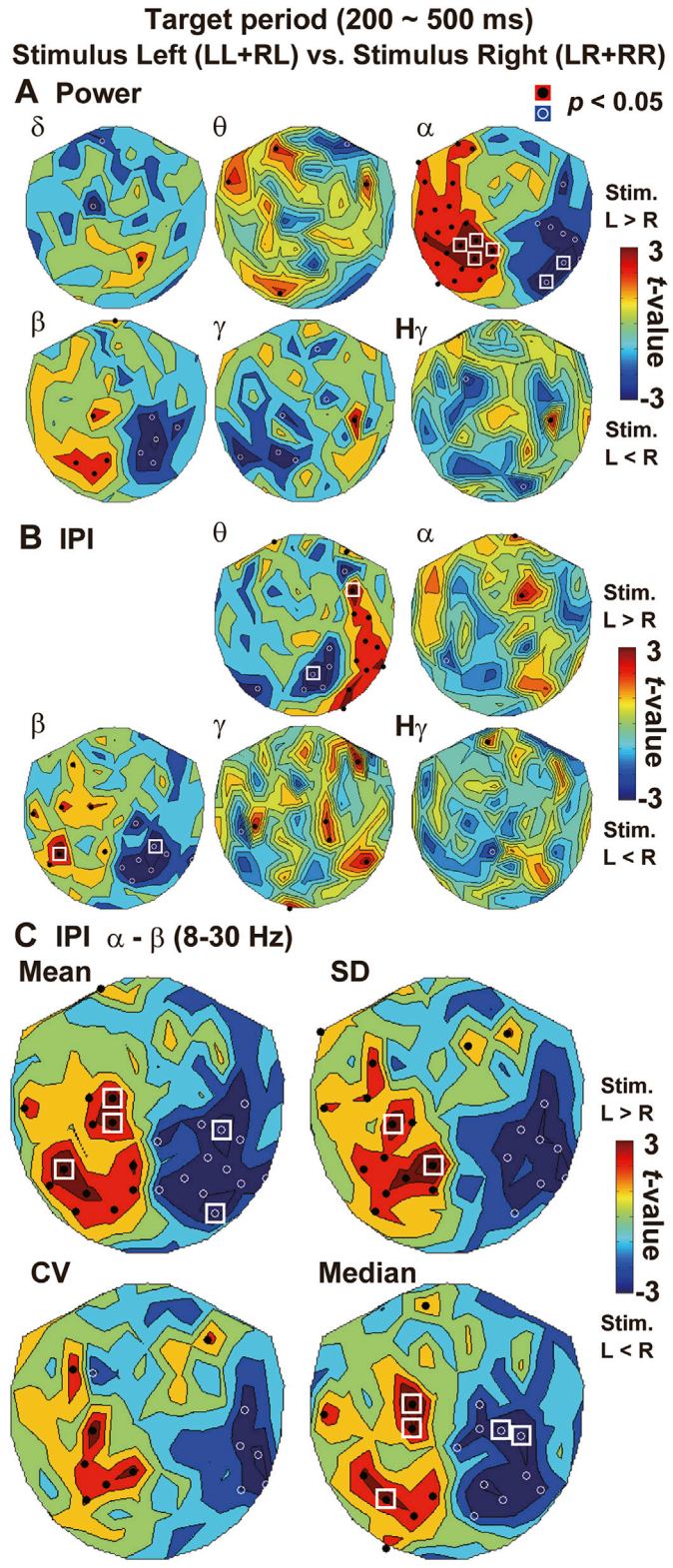

Fig. 7. Changes in powers and IPIs in the target period (200–500 ms). (**A**) Statistical *t*-maps of the power analysis (Stimulus-Left vs. Stimulus-Right). Consistent with previous studies, presenting a visual stimulus induced suppression in alpha and beta bands in the contra-stimulus hemisphere. (**B**) The *t*-maps of mean IPIs separately computed for the six bands. Data in delta band (2–4 Hz) are not shown because the length of a time window (300 ms) was too small to identify delta IPIs. (**C**) The *t*-maps of IPIs in the alpha-to-beta band (8–30 Hz). The IPIs became shorter (mean and median) and more regular (SD and CV) in the contra-stimulus hemisphere.

the inhibition of transient bursts by the decreased alpha/beta power.

Supplementary analyses showed that those results were robust and not influenced by settings of the band-pass filter in the IPI analysis. Fig. S2 displays the results when we used a finite impulse response (FIR) filter, instead of an infinite impulse response (IIR) filter, to identify IPIs. Significant reductions of IPI measures were observed in the contra-attention hemisphere. In Fig. S3, we compared results when an order of the IIR filter (Butterworth, zero-phase) was set at 2, 3, and 4. Attention-related reductions in alpha-to-beta IPIs were observed in all orders, indicating that our results cannot be explained by any contributions of frequency components outside the pass-band (e.g. theta and gamma waves).

3.3. Oscillatory powers and IPIs in the target period

We then analyzed the data in the target period. Presenting a task stimulus induced a decrease in alpha/beta power starting from 200 ms (Fig. 6A), consistent with previous studies (Kulashekhar et al., 2016; Minami et al., 2014). After 500 ms, this decrease was replaced by an increase in power, which reflected an inhibitory control of button-press movements to a non-target grating (see *3.4*). The power suppression from 200 to 500 ms was more clearly seen in the hemisphere contralateral than ipsilateral to a task stimulus (Fig. 6B–D). Since sensor-space *t*-maps of powers between Stimulus-Left (LL + RL) and Stimulus-Right (LR + RR) conditions indicated the contralateral suppression in alpha and beta power (Fig. 7A), we investigated a distribution of IPIs at the six frequency bands (Fig. 7B) and at 8–30 Hz (Fig. 7C). Results reveled that IPIs became faster (mean and median) and more regular (SD and CV) in the contra-stimulus hemisphere.

3.4. NoGo inhibition and an increase in IPIs

Previous studies reported an increase in beta power in the frontal (motor-related) cortex during successful stop trials in Go/NoGo tasks (Jenkinson and Brown, 2011). A recent study further investigated a relationship between an inhibitory control and top-down attention using the spatial-cuing Go/NoGo task (Hong et al., 2017). They found that, while a NoGo stimulus presented in an attended visual field evoked various EEG components related to response inhibition (NoGo-N2 and NoGo-P3), those components were greatly reduced or absent when the NoGo stimulus was presented in an unattended visual field. These previous data indicate that, in the present study, more inhibitory control was necessary when non-target (NoGo) grating appeared in an attended hemifield (LL and RR trials) than when it appeared in an unattended hemifield (LR and RL trials).

Consistent with this prediction, our data in a late target period (500–1000 ms) showed a prominent increase in alpha/beta power in congruent (LL + RR) compared to incongruent (LR + RL) conditions (Fig. 8A). Importantly, this increase was mainly seen in anterior regions of the left hemisphere, which was contralateral to button-press movements (right hand). Results of IPI analysis are displayed in Fig. 8B (six frequency bands) and Fig. 8C (8–30 Hz). We found a significant increase in mean and median IPIs in congruent (inhibitory) compared to incongruent (non-inhibitory) conditions, although no increase was observed in SD or CV (see also Fig. S4 for individual data). Those results showed that neural rhythms in alpha-to-beta band were slowed down in the frontal region when inhibitory control was necessary.

4. Discussion

In contrast to the prediction in **Introduction**, we presently found that the decreased alpha-to-beta power in task-relevant regions was associated with the increased regularity of oscillatory signals. Although regularity (periodicity) of neural oscillation has been measured using autocorrelation analysis (Red'ka and Mayorov, 2015), spectral entropy (Gomez-Pilar et al., 2016; Poza et al., 2012), sample entropy (Gomez and Hornero, 2010), auto-mutual information analysis (Gomez et al., 2007), Q factor (Lemercier et al., 2017), and lagged coherence (Fransen et al., 2015), no study has reported a perception- or attention-related increase in regularity in sensory areas (even an attention-related decrease in regularity of the beta rhythm was reported (Fransen et al., 2015)). We recorded neuromagnetic signals from the human brain at a high sampling rate of 4 kHz, directly depicting a distribution of IPIs. Results revealed that the suppression of alpha/beta power was coupled to reductions in the mean and SD of their IPIs. Those reductions cannot be attributed to a general increase in vigilance or arousal level because they selectively took place in the contralateral hemisphere (bilateral changes would have been observed if they had reflected arousal). Significant reductions were also observed in the median of IPIs, which indicates that our results cannot be explained by an inhibition of transient neural events, e.g. the beta burst (Shin et al., 2017). In contrast to a previous view associating a decrease in oscillation power with uncorrelated behaviors of neural population (Beaman et al., 2017; Pfurtscheller and Lopes da Silva, 1999), our results suggested a new role of the decrease in power to accelerate and regulate brain rhythms in task-relevant regions.

4.1. Dynamic modulation of IPIs linked to cognitive functions

In addition to mean IPI, our data showed significant decreases in SD and CV. Those reductions indicate that basic rhythms in the brain became faster (mean) and more regular (SD) during visual stimulation and attentional allocation. What were neural implications of those changes? One intriguing idea is that those oscillatory signals represent the rhythm of a clock for neural computation (information processing) in the brain. The reduced mean and SD thus suggest that our brain might perceive a stimulus and control attention by regulating and accelerating the neural clock in task relevant regions.

Another interpretation for the increased regularity would be a resolution of dissonance (discordance) in oscillatory signals. It is probable that alpha/beta rhythm over the posterior brain areas emerged not from a unitary source but from multiple sources in the cortex and subcortical regions. Neuromagnetic waveforms recorded at the scalp were thus a mixture of oscillatory signals whose frequencies and phases might be slightly different across source locations. When the signals from most sources are silenced by alpha/beta ERD (Mazaheri and Picton, 2005), this would make signals from remaining sources more regular, resulting in the reduced SD of IPIs.

Finally, changes in IPI measures, especially those in the cue period, might reflect an adjustment of the phase of neural oscillation. It was previously shown that the phase of alpha rhythm in a pre-stimulus interval exerted a significant influence on perceptual outcome of that stimulus (Dugue et al., 2011). Some studies further indicated a top-down control of the oscillation phase toward the optimal processing of an upcoming stimulus (Samaha et al., 2015). Changes in IPIs in a cue period (Fig. 4) might be related to this top-down adjustment of the oscillation phase, because a fixed length of our cue-to-target interval (1 s, Fig. 1) enabled participants to predict an onset of a task stimulus.

Although further research is necessary to elucidate neural mechanism of IPI changes, the present data showed empirical evidence that our brain dynamically adjusts its oscillation on the sub-millisecond scale, depending on sensory inputs and an allocation of attention. These results would provide useful information to refine theories and models about neural mechanisms of perceptual consciousness (Dehaene et al., 2014; Tononi et al., 2016) and attention (Bisley, 2011; Mueller et al., 2017).

4.2. Leading role of beta rhythm in IPI changes

Results on mean IPI computed for each of six frequency bands (Figs. 4A and 7B) revealed a leading role of beta rhythm in modulating IPIs. This indicates that changes in IPIs were *not* a direct consequence of a decrease in power. We found the distinct suppression of alpha power related to attention (LL + LR vs. RL + RR, Fig. 3D) and perception

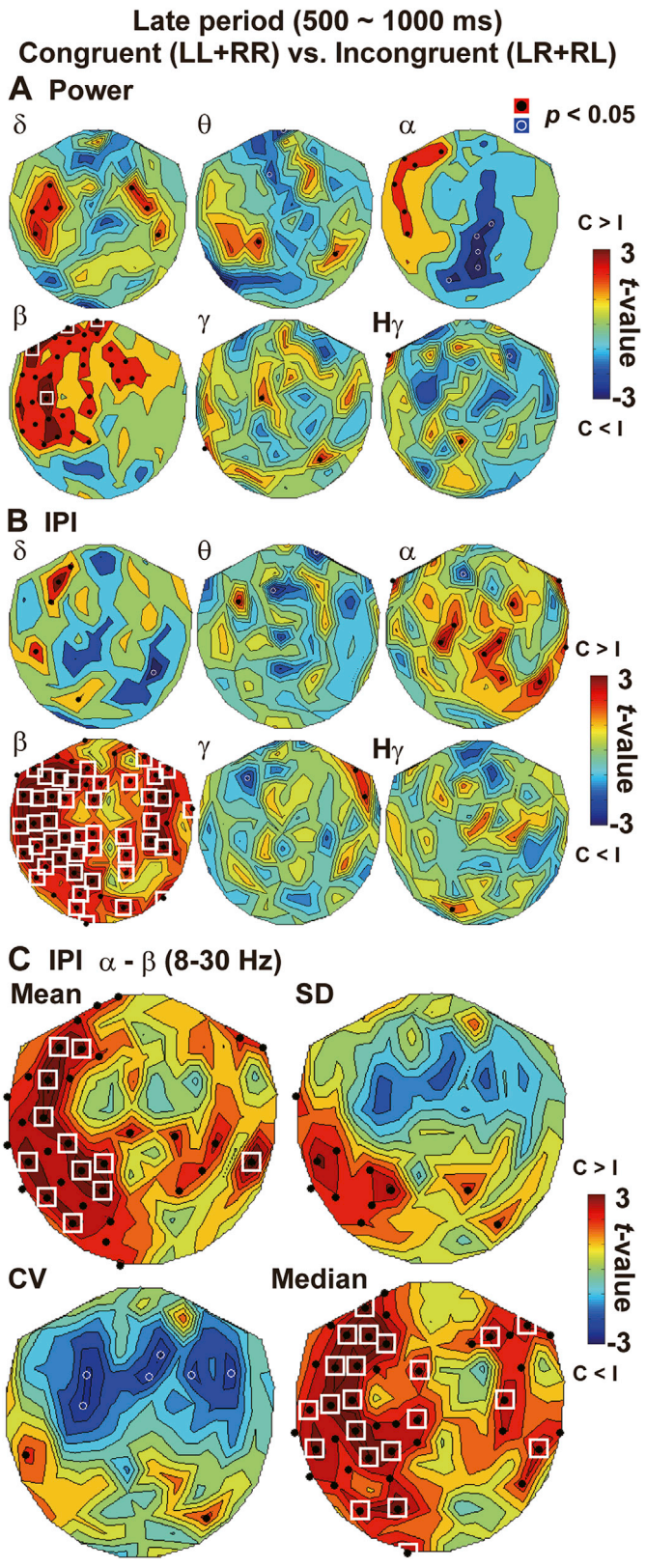

(caption on next column)

Fig. 8. Changes in powers and IPIs related to response inhibition (500–1000 ms). (**A**) The *t*-maps of the power analysis. In congruent trials (LL and RR), a non-target grating was presented at an attended visual field, while it was shown in an unattended field in incongruent trials (LR and RL). Consistent with previous studies (Hong et al., 2017; Jenkinson and Brown, 2011), non-target (No-go) stimulus at the attended hemifield induced neural activity related to response inhibition, as was shown by an increase in beta power (congruent > incongruent, lower left panel) in the frontal cortex contralateral to button-press movements (right hand). (**B**) The *t*-maps of mean IPIs separately computed for the six bands. (**C**) The *t*-maps of IPIs in the alpha-to-beta band (8–30 Hz). An inhibitory control of button-press movements in the congruent trial was associated with an increase in mean and median IPIs. The *p*-values of *t*-tests (congruent vs. incongruent) at a local-maximum sensor over the left frontal region were 0.00033 (mean) and 0.0014 (median). See Fig. S4 for a position of the local-maximum sensor. No change was observed in SDs ($p = 0.50$) or CVs ($p = 0.28$). Those results suggest that the human brain achieved inhibitory control to a non-target stimulus at an attended visual field by slowing down the neural rhythm in the left frontal (motor-related) regions.

(LL + RL vs. LR + RR, Fig. 7A). Nevertheless, those decreases in alpha power elicited no changes in mean IPIs in the same regions (Figs. 4A and 7B), indicating that a change in oscillation amplitude did not necessarily lead to a change in IPIs. In contrast, the perception- and attention-related decrease in beta power was significant but less distinct than alpha band (Figs. 3D and 7A). Those modest changes in beta power, however, were accompanied by significant changes in beta IPIs (Figs. 4A and 7B). In brief, alpha rhythm played a leading role in modulating the amplitude of oscillations, while beta rhythm played a leading role in modulating IPIs. This separation of critical bands (alpha vs. beta) suggests that changes of power and IPIs might be driven by related but non-identical mechanisms of neural oscillation. Compared to other frequency bands, functional roles of beta rhythm remain controversial and unclear (Bressler and Richter, 2015; Engel and Fries, 2010; Spitzer and Haegens, 2017). Our results suggest a new and special role of beta oscillation to orchestrate brain rhythms on a fine temporal scale, in contrast to previous studies focusing on alpha wave (Cohen, 2014; Mierau et al., 2017; Nelli et al., 2017; Wutz et al., 2018).

On the other hand, the present data also showed that beta oscillation was necessary but not sufficient to fully control brain rhythms. The reductions in IPIs were more robustly observed when we investigated MEG waveforms comprising broader frequency components (8–30 Hz, Fig. 4B) than when only the beta band was analyzed (13–30 Hz, Fig. 4A). Although beta wave plays an important role in modulating IPIs, it achieved more stable control of brain rhythms by interacting with other bands of frequencies (e.g. alpha).

Acknowledgments

This work was supported by KAKENHI Grants Number 22680022 and 26700011 from the Japan Society for the Promotion of Science for Young Scientists to Y.N. We thank Mr. Y. Takeshima (National Institute for Physiological Sciences, Japan) for his technical supports. The authors declare no competing financial interest. All data supporting the findings of this study are available from Y.N. upon reasonable request.

Appendix A. Supplementary data

Supplementary data to this article can be found online at https://doi.org/10.1016/j.neuroimage.2019.02.027.

References

Bauer, M., Oostenveld, R., Peeters, M., Fries, P., 2006. Tactile spatial attention enhances gamma-band activity in somatosensory cortex and reduces low-frequency activity in parieto-occipital areas. J. Neurosci. 26, 490–501.

Bauer, M., Stenner, M.P., Friston, K.J., Dolan, R.J., 2014. Attentional modulation of alpha/beta and gamma oscillations reflect functionally distinct processes. J. Neurosci. 34, 16117–16125.

Beaman, C.B., Eagleman, S.L., Dragoi, V., 2017. Sensory coding accuracy and perceptual performance are improved during the desynchronized cortical state. Nat. Commun. 8, 1308.
Benjamini, Y., Hochberg, Y., 1995. Controlling the false discovery rate - a practical and powerful approach to multiple testing. J. Roy. Stat. Soc. B 57, 289–300.
Berger, H., 1929. Uber das Elektrenkephalogramm des Menschen. Arch Psychiat Nervenkr 87, 527–750.
Bisley, J.W., 2011. The neural basis of visual attention. J. Physiol. 589, 49–57.
Brainard, D.H., 1997. The psychophysics toolbox. Spatial Vis. 10, 433–436.
Bressler, S.L., Richter, C.G., 2015. Interareal oscillatory synchronization in top-down neocortical processing. Curr. Opin. Neurobiol. 31, 62–66.
Buzsaki, G., Moser, E.I., 2013. Memory, navigation and theta rhythm in the hippocampal-entorhinal system. Nat. Neurosci. 16, 130–138.
Cirelli, L.K., Bosnyak, D., Manning, F.C., Spinelli, C., Marie, C., Fujioka, T., et al., 2014. Beat-induced fluctuations in auditory cortical beta-band activity: using EEG to measure age-related changes. Front. Psychol. 5, 742.
Cohen, M.X., 2014. Fluctuations in oscillation frequency control spike timing and coordinate neural networks. J. Neurosci. 34, 8988–8998.
de Pesters, A., Coon, W.G., Brunner, P., Gunduz, A., Ritaccio, A.L., Brunet, N.M., et al., 2016. Alpha power indexes task-related networks on large and small scales: a multimodal ECoG study in humans and a non-human primate. Neuroimage 134, 122–131.
Dehaene, S., Charles, L., King, J.R., Marti, S., 2014. Toward a computational theory of conscious processing. Curr. Opin. Neurobiol. 25, 76–84.
Dugue, L., Marque, P., VanRullen, R., 2011. The phase of ongoing oscillations mediates the causal relation between brain excitation and visual perception. J. Neurosci. 31, 11889–11893.
Engel, A.K., Fries, P., 2010. Beta-band oscillations–signalling the status quo? Curr. Opin. Neurobiol. 20, 156–165.
Engel, A.K., Fries, P., Singer, W., 2001. Dynamic predictions: oscillations and synchrony in top-down processing. Nat. Rev. Neurosci. 2, 704–716.
Fransen, A.M., Dimitriadis, G., van Ede, F., Maris, E., 2016. Distinct alpha- and beta-band rhythms over rat somatosensory cortex with similar properties as in humans. J. Neurophysiol. 115, 3030–3044.
Fransen, A.M., van Ede, F., Maris, E., 2015. Identifying neuronal oscillations using rhythmicity. Neuroimage 118, 256–267.
Fries, P., 2005. A mechanism for cognitive dynamics: neuronal communication through neuronal coherence. Trends Cognit. Sci. 9, 474–480.
Fries, P., 2009. Neuronal gamma-band synchronization as a fundamental process in cortical computation. Annu. Rev. Neurosci. 32, 209–224.
Fujioka, T., Ross, B., Trainor, L.J., 2015. Beta-band oscillations represent auditory beat and its metrical hierarchy in perception and imagery. J. Neurosci. 35, 15187–15198.
Gomez-Pilar, J., Martin-Santiago, O., Suazo, V., de Azua, S.R., Haidar, M.K., Gallardo, R., et al., 2016. Association between EEG modulation, psychotic-like experiences and cognitive performance in the general population. Psychiatr. Clin. Neurosci. 70, 286–294.
Gomez, C., Hornero, R., 2010. Entropy and complexity analyses in Alzheimer's disease: an MEG study. Open Biomed. Eng. J. 4, 223–235.
Gomez, C., Hornero, R., Abasolo, D., Fernandez, A., Escudero, J., 2007. Analysis of the magnetoencephalogram background activity in Alzheimer's disease patients with auto-mutual information. Comput. Methods Progr. Biomed. 87, 239–247.
Hong, X., Wang, Y., Sun, J., Li, C., Tong, S., 2017. Segregating top-down selective attention from response inhibition in a spatial cueing go/NoGo task: an ERP and source localization study. Sci. Rep. 7, 9662.
Jenkinson, N., Brown, P., 2011. New insights into the relationship between dopamine, beta oscillations and motor function. Trends Neurosci. 34, 611–618.
Jensen, O., Kaiser, J., Lachaux, J.P., 2007. Human gamma-frequency oscillations associated with attention and memory. Trends Neurosci. 30, 317–324.
Jensen, O., Mazaheri, A., 2010. Shaping functional architecture by oscillatory alpha activity: gating by inhibition. Front. Hum. Neurosci. 4, 186.
Klimesch, W., 2012. alpha-band oscillations, attention, and controlled access to stored information. Trends Cognit. Sci. 16, 606–617.
Knyazev, G.G., 2007. Motivation, emotion, and their inhibitory control mirrored in brain oscillations. Neurosci. Biobehav. Rev. 31, 377–395.
Kulashekhar, S., Pekkola, J., Palva, J.M., Palva, S., 2016. The role of cortical beta oscillations in time estimation. Hum. Brain Mapp. 37, 3262–3281.
Lemercier, C.E., Holman, C., Gerevich, Z., 2017. Aberrant alpha and gamma oscillations ex vivo after single application of the NMDA receptor antagonist MK-801. Schizophr. Res. 188, 118–124.
Mazaheri, A., Picton, T.W., 2005. EEG spectral dynamics during discrimination of auditory and visual targets. Brain Res Cogn Brain Res 24, 81–96.
Mierau, A., Klimesch, W., Lefebvre, J., 2017. State-dependent alpha peak frequency shifts: experimental evidence, potential mechanisms and functional implications. Neuroscience 360, 146–154.
Minami, T., Noritake, Y., Nakauchi, S., 2014. Decreased beta-band activity is correlated with disambiguation of hidden figures. Neuropsychologia 56, 9–16.
Mueller, A., Hong, D.S., Shepard, S., Moore, T., 2017. Linking ADHD to the neural circuitry of attention. Trends Cognit. Sci. 21, 474–488.
Nelli, S., Itthipuripat, S., Srinivasan, R., Serences, J.T., 2017. Fluctuations in instantaneous frequency predict alpha amplitude during visual perception. Nat. Commun. 8, 2071.
Nishitani, N., Hari, R., 2002. Viewing lip forms: cortical dynamics. Neuron 36, 1211–1220.
Noguchi, Y., Kimijima, S., Kakigi, R., 2015. Direct behavioral and neural evidence for an offset-triggered conscious perception. Cortex 65, 159–172.
Osipova, D., Takashima, A., Oostenveld, R., Fernandez, G., Maris, E., Jensen, O., 2006. Theta and gamma oscillations predict encoding and retrieval of declarative memory. J. Neurosci. 26, 7523–7531.
Palva, S., Palva, J.M., 2011. Functional roles of alpha-band phase synchronization in local and large-scale cortical networks. Front. Psychol. 2, 204.
Pelli, D.G., 1997. The VideoToolbox software for visual psychophysics: transforming numbers into movies. Spatial Vis. 10, 437–442.
Pfurtscheller, G., Lopes da Silva, F.H., 1999. Event-related EEG/MEG synchronization and desynchronization: basic principles. Clin. Neurophysiol. 110, 1842–1857.
Poza, J., Gomez, C., Bachiller, A., Hornero, R., 2012. Spectral and non-linear analyses of spontaneous magnetoencephalographic activity in Alzheimer's disease. J Healthc Eng 3, 299–321.
Red'ka, I.V., Mayorov, O.Y., 2015. Effect of restriction of visual afferentation on the rhythmic organization of alpha EEG activity. Neurophysiology 47, 225–233.
Samaha, J., Bauer, P., Cimaroli, S., Postle, B.R., 2015. Top-down control of the phase of alpha-band oscillations as a mechanism for temporal prediction. Proc. Natl. Acad. Sci. U. S. A. 112, 8439–8444.
Shin, H., Law, R., Tsutsui, S., Moore, C.I., Jones, S.R., 2017. The rate of transient beta frequency events predicts behavior across tasks and species. Elife 6.
Spitzer, B., Haegens, S., 2017. Beyond the status quo: a role for beta oscillations in endogenous content (Re)activation. eNeuro 4.
Suzuki, M., Noguchi, Y., Kakigi, R., 2014. Temporal dynamics of neural activity underlying unconscious processing of manipulable objects. Cortex 50, 100–114.
Tadel, F., Baillet, S., Mosher, J.C., Pantazis, D., Leahy, R.M., 2011. Brainstorm: a user-friendly application for MEG/EEG analysis. Comput. Intell. Neurosci. 2011, 879716.
Taube, J.S., 2010. Interspike interval analyses reveal irregular firing patterns at short, but not long, intervals in rat head direction cells. J. Neurophysiol. 104, 1635–1648.
Tononi, G., Boly, M., Massimini, M., Koch, C., 2016. Integrated information theory: from consciousness to its physical substrate. Nat. Rev. Neurosci. 17, 450–461.
van Ede, F., Koster, M., Maris, E., 2012. Beyond establishing involvement: quantifying the contribution of anticipatory alpha- and beta-band suppression to perceptual improvement with attention. J. Neurophysiol. 108, 2352–2362.
Werkle-Bergner, M., Grandy, T.H., Chicherio, C., Schmiedek, F., Lovden, M., Lindenberger, U., 2014. Coordinated within-trial dynamics of low-frequency neural rhythms controls evidence accumulation. J. Neurosci. 34, 8519–8528.
Worden, M.S., Foxe, J.J., Wang, N., Simpson, G.V., 2000. Anticipatory biasing of visuospatial attention indexed by retinotopically specific alpha-band electroencephalography increases over occipital cortex. J. Neurosci. 20, RC63.
Wutz, A., Melcher, D., Samaha, J., 2018. Frequency modulation of neural oscillations according to visual task demands. Proc. Natl. Acad. Sci. U. S. A. 115, 1346–1351.
Wyart, V., Tallon-Baudry, C., 2009. How ongoing fluctuations in human visual cortex predict perceptual awareness: baseline shift versus decision bias. J. Neurosci. 29, 8715–8725.